J Nanopart Res (2023) 25:254
https://doi.org/10.1007/s11051-023-05903-2

RESEARCH PAPER

Engineering micro/nano-fibrous scaffolds with silver coating for tailored wound repair applications

Parvathalu Kalakonda · Shalini Thudumu · Soujanya Laxmi Mynepally · Pritam Mandal · Sreenivas Banne · Pranay Bhaskar Kalakonda · Bala Bhaskar Podili

Received: 29 September 2023 / Accepted: 24 November 2023

Abstract Electrospun scaffolds originating from polymeric amalgams, specifically poly(glycerol sebacate/poly(ε-caprolactone) (PGS/PCL) and poly(methyl methacrylate)–poly(ε-caprolactone) (PMMA/PCL), have emerged as a versatile substrate within the realm of biomedical tissue engineering. Their salience is underscored by their remarkable thermal, optical, and mechanical attributes. In this investigation, we harnessed conventional electro-spinning methodologies to fabricate nano/micro-fibrous scaffolds from a hybrid composite, amalgamating PMMA/PCL and PGS/PCL fibers. A pivotal innovation lay in the precise deposition of silver nanoparticles (AgNPs) on one facet of these scaffolds, endowing them with anti-bacterial functionality. This AgNP coating not only forestalled melting proclivities but also meticulously tuned structural facets, engendering a diminution in pore diameter and augmentation in fiber diameter, thereby engendering an elevation in thermo-mechanical performance. Comparative scrutiny delineated that the PMMA/PCL composite fibrous scaffolds manifested superior mechanical attributes, including augmented modulus (*E*) and ultimate tensile strength (UTS), accompanied by attenuated tensile strain, obviating the requisite for supplementary post-processing steps. These AgNP-endowed composite fibrous scaffolds engender sanguine prospects for biomedical applications, encompassing surgical meshes, bandages, and band-aids, underpinned by their amplified anti-bacterial characteristics, which are instrumental in the context of wound healing.

Keywords Fibrous scaffold · Electro-spun fibers · Mechanical properties · Silver Nanoparticles · Nanobiomedicine · Nanocoposites

P. Kalakonda (✉) · S. Thudumu · S. . Mynepally · B. B. Podili
Department of Physics, Government City UG/PG College (A), Nayapul, Osmania University, Hyderabad 500002, Telangana, India
e-mail: parvathalu.k@gmail.com; parvathalu.ce@telangana.gov.in; pkalakon@andrew.cmu.edu

P. Mandal
Department of Physics, Michigan Technological University, Houghton, MI 4993, USA

S. Banne
Department of Chemistry and Biosciences, Rice University-BRC, Houston, TX 77005, USA

P. B. Kalakonda
Department of Materials Science and Engineering, North Carolina State University, Raleigh, NC 27695, USA

Introduction

Chronic wounds and burns are emerging as a significant public health concern. Recent research indicates that over 5 million individuals in the USA alone suffer from chronic wounds [1, 2]. The skin, our body's largest organ, plays a pivotal role in numerous vital biological functions and serves as the primary

Published online: 11 December 2023

defense against environmental pathogens. The skin barrier's integrity is compromised, then the vulnerability to microbial infections increases [3, 4]. These infections pose a formidable obstacle to effective wound healing by creating a conducive environment for bacterial proliferation. However, this challenge can be effectively addressed through the application of wound dressings composed of fabricated AgNP-coated composite fibrous scaffolds, harnessing the potent anti-microbial properties of AgNPs [5, 6].

Previously, natural polymers like gelatin and collagen, along with their nanocomposites, have found applications in the biomedical field [7–9]. A nanocomposite incorporating gelatin and silver nanoparticles emerged as a promising material for anti-bacterial purposes. Notably, this nanocomposite exhibited anti-microbial properties against a diverse range of bacterial strains, including *Escherichia coli*, *Staphylococcus aureus*, and *Bacillus cereus* [10, 11]. Interestingly, it demonstrated more pronounced anti-bacterial activity against Gram-positive pathogens compared to Gram-negative ones. While metal nanoparticles have been integrated into wound and burn dressings to curb microbial activity [12, 13], they proved less effective than silver nanoparticles due to their lack of foldable behavior, a crucial requirement for efficient wound dressing applications. In this context, synthetic polymer scaffolds have assumed a crucial role in wound dressing owing to their exceptional flexibility and biocompatibility. Synthetic polymers offer superior mechanical properties when compared to hydrogel materials. Electro-spun scaffolds, in particular, exhibit favorable morphological characteristics, rendering them excellent candidates for use in tissue engineering and wound healing applications [14, 15].

PGS has gained recognition as a prospective biopolymer for developing hybrid scaffolds in biomedical applications, thanks to its unique thermo-mechanical and biological properties [16–19]. Notably, PGS's functional groups are FDA-approved, making it an attractive biomaterial [19]. Its elastomeric nature, ease of synthesis, high biodegradability, and biocompatibility position PGS as a promising candidate for industrial tissue engineering applications [21–32]. While PGS/PCL composite scaffolds have shown significant cellular responses in biocompatibility tests, pristine PGS with low molecular weights is unsuitable for electro-spinning fabrication. To address this, PGS nanofiber formation can be achieved by incorporating other polymers like gelatin, poly(ε-caprolactone) (PCL), and polymethyl methacrylate (PMMA). PCL and PMMA, with their FDA-approved status, are biodegradable yet hydrophobic, resulting in poor cell attachment. Nevertheless, these polymers possess unique physical properties. Coating scaffolds with AgNPs, known for their anti-bacterial activity, can enhance anti-microbial properties and inhibit bacterial colonization in wound healing applications [19, 55, 56]. Creating micron-sized fibrous scaffolds with silver nanoparticles and desirable thermo-mechanical characteristics is vital for the biomaterial industry [33–43]. Previous studies have explored nano-coatings of anti-bacterial materials, like metal nanoparticles and antibiotics, on micro/nano-fibrous scaffolds to combat microbial infections. However, concerns about the release of nano-coatings and potential toxicity have arisen [44–46]. Given the prevalence of microbial infections in medical procedures and wound healing, designing scaffolds with anti-bacterial coatings is essential for tissue engineering and wound care. Our focus is on investigating the potential of composite scaffolds with anti-bacterial activity, serving as effective tissue engineering skin grafts for wound and burn treatments.

In this work, we fabricated PGS/PCL, PMMA/PCL composite scaffold samples by the electrospinning process. These nano-composite scaffolds are found to be stable without any further post-processing treatment [32]. The 1:1 ratio of PGS/PCL and PGS/PMMA shows better mechanical properties compared to other reported combinations [47–50]. We coat the scaffolds with silver nanoparticles AgNPs on the surface of fiber scaffolds and measure their thermal, mechanical, and compositional activity. We find the AgNP coating on the surface of the scaffold enhances their mechanical properties, viscoelastic properties, and thermal stability, and acts as desirable anti-bacterial agents for biomedical applications. The electro-spun synthesized scaffolds exhibit superiority over conventional options in terms of anti-bacterial efficacy, tailored properties, biocompatibility, structure, degradation control, and versatility. This places them at the forefront of advanced materials for diverse applications, offering a compelling alternative to traditional scaffolds in the biomedical and materials science domains.

Methods and characterization

Materials

We sourced the chemicals, including PGS, PCL, and PMMA, as well as the solvents chloroform and ethanol, from Sigma-Aldrich. The chemical structures of PGS, PCL, and PMMA are illustrated in Fig. 1. Subsequently, we prepared solutions by dissolving PGS and PCL, as well as PMMA and PCL blends, in a 1:1 ratio using chloroform to ethanol mixture (9:1). These solutions were prepared at a polymer concentration of 20% (w/v). To ensure a homogeneous mixture, we allowed the solutions to adequately mix over approximately 10 h at room temperature before proceeding with the electro-spinning process.

Electro spinning

The blends of PGS and PCL (with a molecular weight of 80,000 g/mol) were dissolved in a solvent mixture of chloroform and ethanol (9:1) at a 1:1 ratio. Keeping the co-polymer concentration consistent at 20% (w/v) for all constructs, the solutions underwent thorough mixing for 5 h at 80 °C before the electro-spinning process. The prepared solution was loaded into a 5-mL syringe (Becton-Dickinson, Franklin Lakes, NJ, USA). A 20-gauge blunt metallic needle (NANON Supply, MECC, Fukuoka, Japan) was affixed to the syringe, connected to 10–15 cm of Teflon tubing (Cole-Parmer Instrument Company, Vernon Hills, IL, USA). Employing an electrical field of 19.5 kV over a distance of 15 cm, the co-polymer solution was consistently dispensed at a flow rate of 0.9 mL/h during the electro-spinning process, lasting 3 h and resulting in a sheet thickness of 450–500 µm. Subsequently, the electro-spun sheet underwent final drying overnight under the electro-spinning system fan, facilitating solvent evaporation.

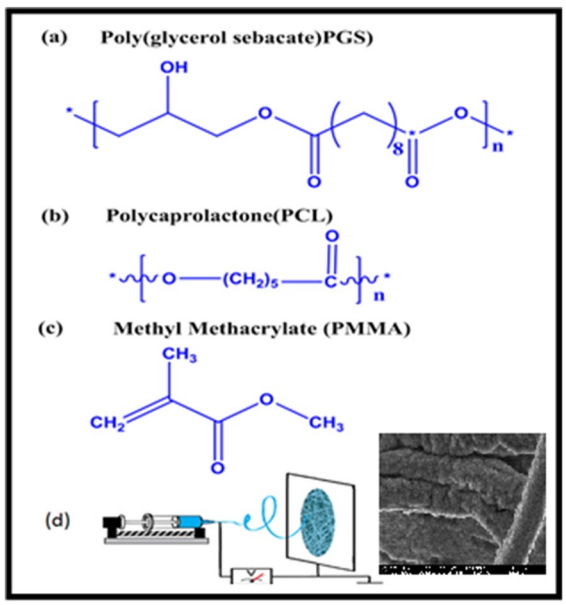

Fig. 1 **a** Molecular structure of PGS showcasing ester bonds and alkaline groups. **b** Molecular structure of PCL highlighting ester bonds. **c** Molecular structure of PMMA emphasizing ester bonds. **d** Schematic representation of a typical electro-spinning design

RF sputtering-fiber coating

Utilizing an RF magnetron sputtering technique (DC/RF Magnetron Sputter System, Syskey Technologies, Xinfeng Township, Taiwan), silver (Ag) patterns were meticulously fabricated. A high-purity Ag target (99.999%, 3×0.6 in) served as the material source. To delineate the patterns, a laser cutter-prepared shadow mask was strategically positioned over the electro-spun sheets before the sputtering process. The creation of the nano-crystalline Ag coating involved generating a plasma within the chamber using argon gas at a flow rate of 20 sccm and an RF power of 100 watts, with base and operating pressures adjusted to 1×10^{-6} and 5×10^{-3} Torr, respectively. Key parameters, including substrate rotation, target–substrate distance, and sputtering time, were set at 15 rpm, 14 cm, and 1000 s, respectively. The film thickness was modulated by varying the sputtering time.

Mechanical characterization

We assessed the mechanical properties using the DMA 800 system from TA Instruments, maintaining a constant room temperature and employing a 5 N load cell at a testing rate of 1 mm/s. The scaffold was subjected to temperature scanning from 25 to 100 °C with a ramp rate of 2 °C/min [52–54]. The tensile stress (σ) was measured as a function of tensile strain (ε) at a rate of 1 N/min, in accordance with ASTM standard 882, including the testing of plastic sheets with a thickness of less than 0.25 mm.

Thermal analysis

We employed a differential scanning calorimetry (DSC-204 by Netzsch) to gauge heat capacity and the heating/cooling profiles of the scaffolds. This analysis was conducted at a heating rate of 30 °C/min. Additionally, to evaluate the thermal stability of the AgNP-coated scaffolds, we utilized thermogravimetric analysis (TGA-209F by Netzsch) under atmospheric N2 conditions. The assessment spanned a temperature range from 270 to 800 °C, with a heating rate of 3 °C/min.

Microstructure characterization

We conducted an in-depth examination of the morphology of the hybrid composite fibrous scaffold using high-resolution scanning electron microscopy (HR-SEM) with a Nova Nano 630 instrument.

FTIR

To discern the chemical compositions and functional groups within the nano-composite fibrous scaffold, we performed Fourier transform infrared spectroscopy (FTIR) analysis using an FTIR-6700 instrument, covering a range from 4000 cm^{-1} to 400 cm^{-1}.

ICP-OES

To quantify the activity of Ag+ions released into deionized water (DI) as a crucial component of their antibacterial efficacy, we employed inductively coupled plasma optical emission spectrometry (ICP-OES).

Results and discussion

In this study, we employed electro-spinning (Fig. 1) to fabricate micro/nano fibrous scaffolds using a blend of PGS/PCL (1:1) and PMMA/PCL. Subsequently, these scaffolds were precisely coated with a 150-nm-thick layer of silver nanoparticles (AgNPs) via controlled RF sputtering. The electro-spinning method obviated the need for additional post-processing. A critical challenge in the sputtering process was to prevent substrate temperature from rising significantly, as elevated temperatures could potentially cause the PCL-based composite scaffolds to melt due to their glass transition below 60 °C. Our procedure successfully maintained the substrate temperature below 40 °C, ensuring the prevention of PCL polymer melting. This temperature control facilitated improved adhesion of AgNPs to the polymer, consequently enhancing the scaffold's thermo-mechanical properties. The mechanical characteristics of the scaffold materials are closely linked to both the scaffold's microstructure and the presence of the AgNP coating. RF sputtering offered precise control over the thickness of the AgNP coating. In addition to fabricating AgNP-coated nano-composite scaffolds comprising PGS/PCL and PMMA/PCL, this study encompassed a comprehensive comparison of their thermo-mechanical properties with those of other reported nano-composite scaffolds [19, 49]. These AgNP coatings are anticipated to serve as potent anti-bacterial agents, making these scaffolds suitable for diverse applications, including band-aids, elastic heaters, strain gauges, temperature sensors, and flexible electronic devices.

FTIR analysis (Fig. 2) was conducted to assess the chemical composition of the composite fibrous scaffolds. The functional groups of PGS and PMMA polymers were found to overlap with PCL polymer bands. Notably, two prominent bands were identified: one at 1723 cm^{-1}, corresponding to the stretching vibration of carboxyl (C=O), and the other at 1167 cm^{-1}, attributed to the stretching vibration of the ether group (C–O) in the spectrum. Additional stretching bands were observed, including symmetric

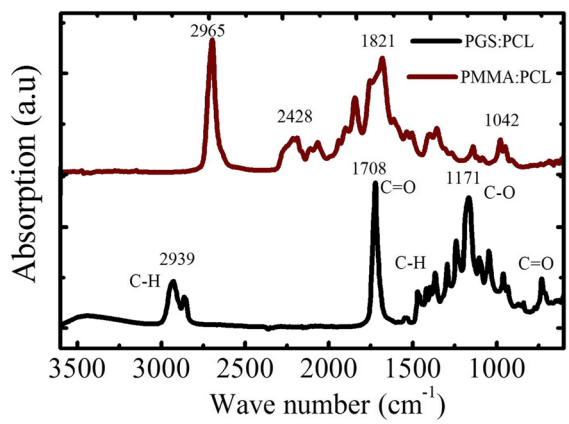

Fig. 2 FTIR spectra of the fibrous scaffold of PGS/PCL and PMMA/PCL

C–H stretching at 2926 cm^{-1}, as well as C–O and C–C stretching vibrations at 1295 cm^{-1}. Methyl groups exhibited stretching characteristics at 1360, 2930, and 2860 cm^{-1}, while the ester band C–O vibration was evident at 1166, 1723, 930, and 1287 cm^{-1}. The FTIR analysis confirmed the persistence of PGS, PCL, and PMMA polymer characteristics, albeit with a reduction in their microstructure. Despite the thinness of the scaffold films, the functional attributes of these polymers remained intact, indicating their suitability for hosting surface-active materials.

Figure 3A displays the surface morphology of both fibrous scaffolds. The scaffold's diameter and porosity significantly influence its mechanical properties. The application of 150-nm-thick Ag coatings on the scaffold fibers enhances mechanical characteristics

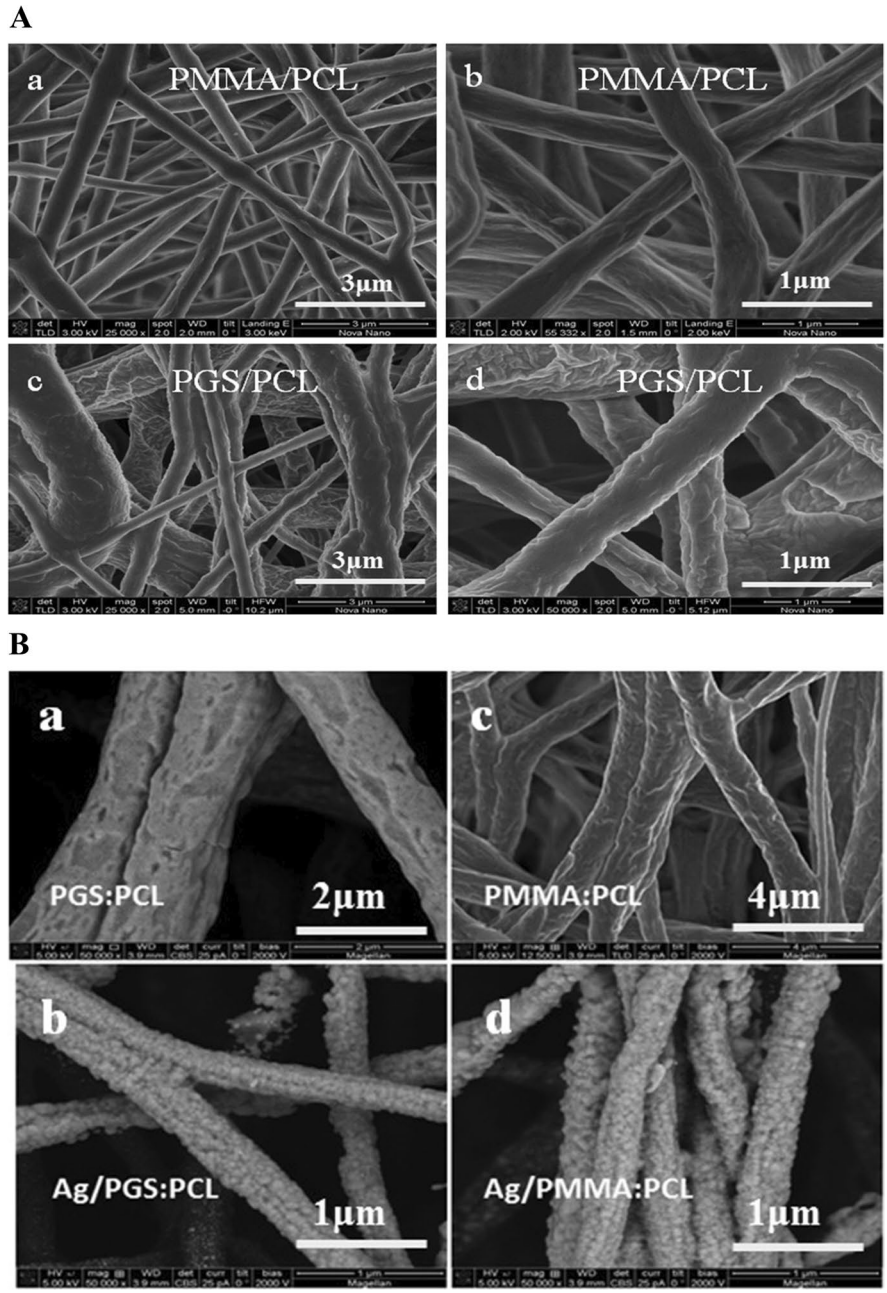

Fig. 3 **A** Scanning electron microscopy (SEM) images illustrating the pristine fibrous morphology of **a** and **b** PMMA/PCL scaffolds, as well as (**c**) and (**d**) PGS/PCL scaffolds at different resolutions. **B**. SEM images of the pristine fibrous **a** PGS/PCL, **c** PMMA/PCL scaffold and AgNP-coated fibrous scaffolds, **b** 150-nm-AgNP-PGS/PCL, and **d** 150-nm-AgNP-PMMA/PCL. **C**. SEM images of the pristine fibrous **a** PGS/PCL, **b** PMMA/PCL scaffolds. Pristine fibrous scaffold distribution of diameter **c** PGS/PCL and **d** PMMA/PCL

Fig. 3 (continued)

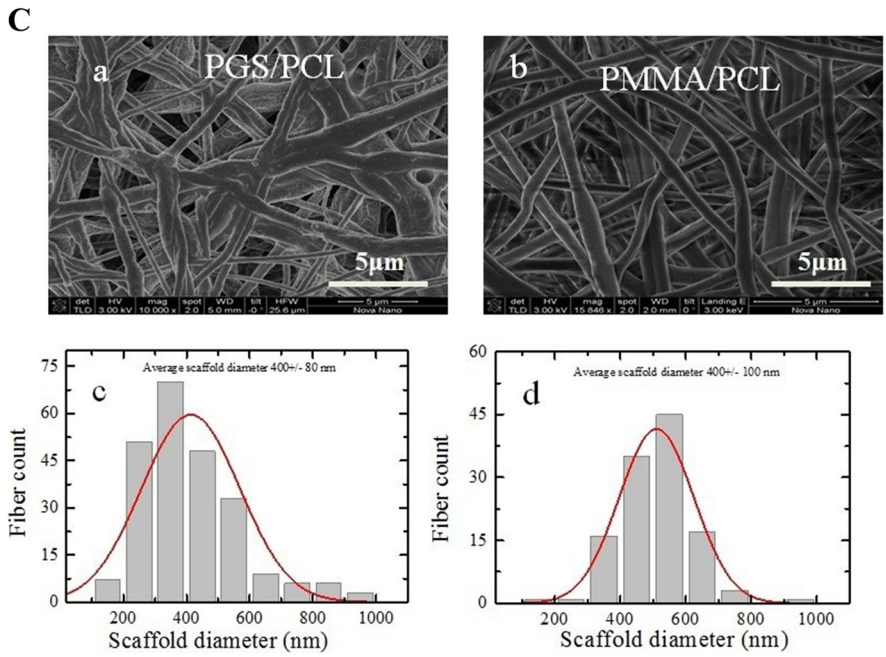

by reducing pore size, increasing diameter, and promoting stronger interfacial interactions between the scaffold fiber and silver nanoparticles (Fig. 3B). The diameter of the pristine scaffolds, as determined through statistical analysis of SEM images using ImageJ Software, was measured at 400 nm (Fig. 3C). Following AgNP coating on the scaffolds, there is an observed increase in the diameter of the fibrous scaffolds alongside a reduction in pore size.

Mechanical characteristics were assessed for fibrous scaffolds both with and without the presence of silver nanoparticle (AgNP) coating. These rectangular-shaped scaffolds had an average thickness ranging from 100 to 200 µm. In Fig. 4A, the inset displays the linear region of the stress-strain curve for both scaffold types within the 10–15% strain range. The mechanical attributes of the scaffolds are contingent on microstructural parameters such as fiber diameter, pore diameter, and the presence of metal coating. The tensile modulus for pristine PGS/PCL (1:1) scaffolds measured approximately 3.3 MPa, while that of PMMA/PCL scaffolds reached approximately

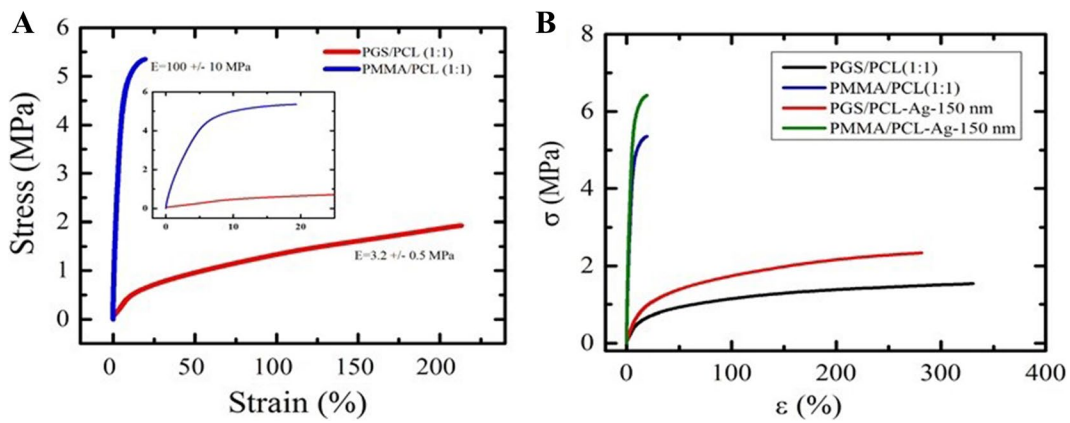

Fig. 4 **A** The tensile stress (σ) versus tensile strain (ϵ) of fibrous scaffold of PGS/PCL and PMMA/PCL; **B** the tensile stress (σ) versus tensile strain (ϵ) of the fibrous scaffold of Ag-coated PGS/PCL and PMMA/PCL

100 MPa. Notably, the mechanical properties of AgNP-coated scaffolds exhibited a substantial increase, approximately 3–4 times higher than those of the pristine scaffolds (Fig. 4B).

The pristine PMMA/PCL scaffold demonstrated an impressive ultimate tensile strength (UTS), surpassing that of the pristine PGS/PCL polymer scaffold by approximately 30-fold. Intriguingly, the tensile strain exhibited a substantial increase of approximately 250% for the PGS/PCL scaffold, whereas the PMMA/PCL scaffold experienced a more modest 25% strain (Fig. 4B). This difference in mechanical behavior may be attributed to the AgNP coating, which potentially renders the scaffold more brittle due to enhanced interfacial interactions between AgNPs and the scaffold fiber. Comparatively, the PMMA/PCL fibrous scaffold exhibited a higher modulus (*E*), elevated UTS, and increased stiffness when contrasted with the PGS/PCL fibrous scaffold. This improvement can be attributed to the tightly packed morphological structure of the PMMA/PCL scaffold, characterized by a larger diameter (Fig. 2C). The difference in mechanical behavior between the two scaffolds, both featuring AgNPs, can be attributed to the influence of the AgNP coating on the scaffold's properties. The heightened brittleness observed may result from increased interfacial interactions between AgNPs and the scaffold fibers. The presence of AgNPs appears to impact tensile strength, potentially altering structural integrity or interactions among scaffold components. A more in-depth exploration into the specific nature of these interactions and their effects on mechanical properties is warranted to gain a thorough understanding of the distinct behaviors observed in the two scaffolds. Morphological alterations in the scaffold fiber post-mechanical testing are depicted in Fig. 5. The PGS/PCL scaffold fiber displayed twisting and stretching behavior, whereas the PMMA/PCL scaffold exhibited less twisting and a tape-like stretching pattern. In light of these findings, it becomes evident that the PMMA/PCL scaffold holds promise as a material suitable for an expanded range of wound healing applications. We postulate that the substantial enhancement in mechanical properties following AgNP coating is primarily attributable to increased friction between the fibers. This phenomenon may also be attributed to the interlocking of fibers, preventing slippage and amplifying the friction between adjacent fibers, particularly evident on the fiber surface.

The introduction of Ag coating had a profound impact on the thermal behavior of the micro-scaffold fiber, influencing the melting and glass transition temperatures. We evaluated these thermal characteristics using the DMA technique (Fig. 6). The scaffold was subjected to temperature scanning from 25 to 100 °C with a ramp rate of 2 °C/min. Both pristine fibrous scaffolds exhibited a broader glass transition temperature ranging from 60 to 90 °C. Noticeably, the storage modulus (*E′*) exhibited considerably higher values for PMMA/PCL and Ag-PMMA/PCL when compared to the fibrous scaffolds of PGS/PCL and Ag-PGS/PCL, as depicted in Fig. 6A. This difference can be attributed to the heat transfer between the fibers and the AgNP coating. Both pristine scaffold samples commenced fracturing at lower temperatures, primarily due to the melting of fibers. In contrast, the mechanical fracture of Ag-coated scaffolds occurred at higher temperatures, indicating that Ag improve the mechanical integrity of the pristine scaffold. The

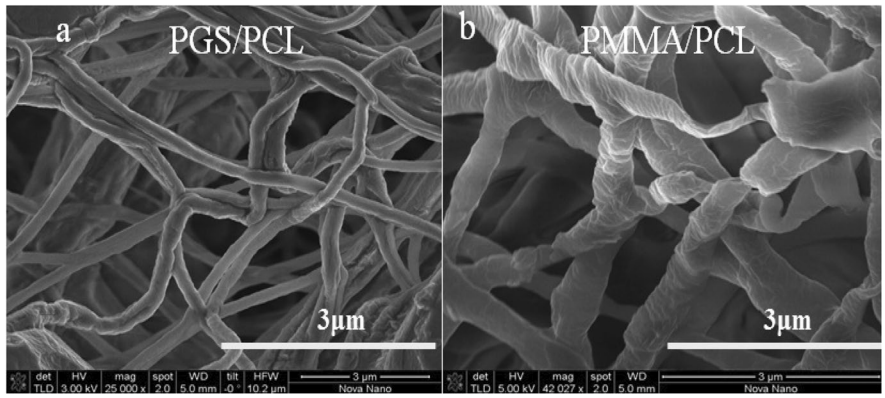

Fig. 5 SEM images of the pristine fibrous PGS/PCL and PMMA/PCL scaffolds after mechanical testing

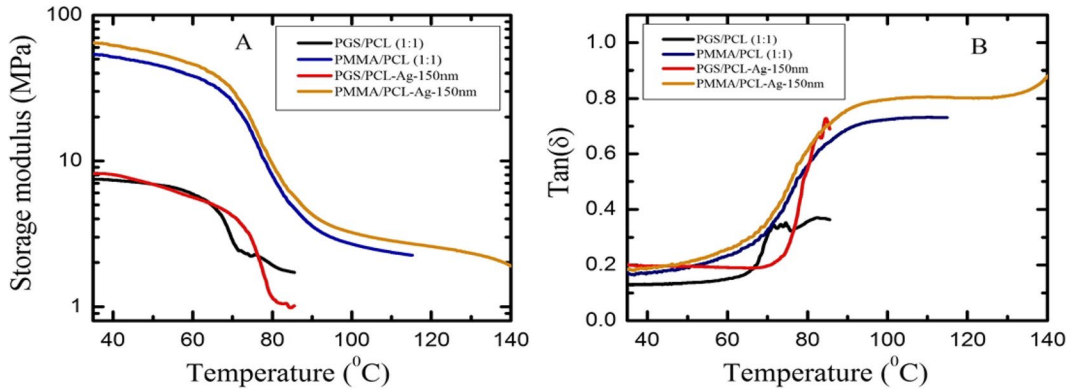

Fig. 6 **A** The storage modulus is a function of temperature measurements for both PGS/PCL and PMMA/PCL scaffolds. **B** Damping ratio (tan δ) versus temperature measurements for both PGS/PCL and PMMA/PCL scaffolds

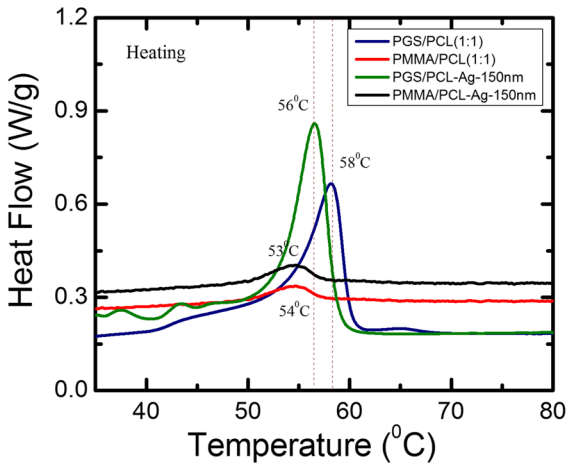

Fig. 7 Differential scanning calorimetry measurements of pristine and Ag-coated fibrous scaffold of PGS/PCL, PMMA/PCL

Ag coating effectively restricted fiber motion, resulting in increased scaffold stiffness and, consequently, mechanical reinforcement.

To decipher the underlying mechanism behind the mechanical enhancements observed in both fibrous scaffolds and Ag-coated scaffolds, we employed differential scanning calorimetry (DSC). This analysis allowed us to investigate the crystalline behavior and stiffness of the scaffolds, both of which contribute to the enhancement of modulus (*E*) and a reduction in melting temperature (Tm). Our findings revealed a distinct and sharp melting peak at 58 °C for PGS/PCL and 54 °C for PMMA.PCL (Fig. 7), indicating a decrease in the melting temperature of both Ag-coated scaffolds by approximately 1 °C for PGS/PCL and 4 °C for PMMA/PCL. Additionally, the endothermic peak exhibited a slight increase in the Ag-coated fibrous scaffold, signifying heightened crystalline behavior. This increase can be attributed to the restricted thermal motion of microfibers and the micro/nano-confinement imposed by the Ag coating. The broad and closely aligned glass transition temperature of the micro-fibrous scaffold, as determined from DSC and corroborated by DMA measurements, further supports these observations.

Thermal stability assessments of both fibrous scaffolds were conducted using TGA technique, as illustrated in Fig. 8. In the Ag-coated fibrous scaffold, the mass degradation associated with burning off was notably reduced. This reduction in mass degradation is likely attributed to the heat transfer from silver nanoparticles to the fibers, resulting in stronger interfacial interactions. The mass loss profiles of the scaffolds exhibited two distinct regimes, possibly indicative of the temperature-dependent degradation of the two polymers that phase separate prior to complete degradation. The improved thermal stability observed in both Ag-coated scaffolds was manifested by an increase of approximately 100 °C in the onset of degradation temperature. Remarkably, even at 800 °C, the Ag-coated sample retained 10% of its initial weight, potentially owing to the nano-confinement effect imparted by the Ag coating on the micro-scaffold composites.

We underscore the potential of silver nanoparticles (AgNPs) for wound healing applications owing to their robust antibacterial activity. To assess the

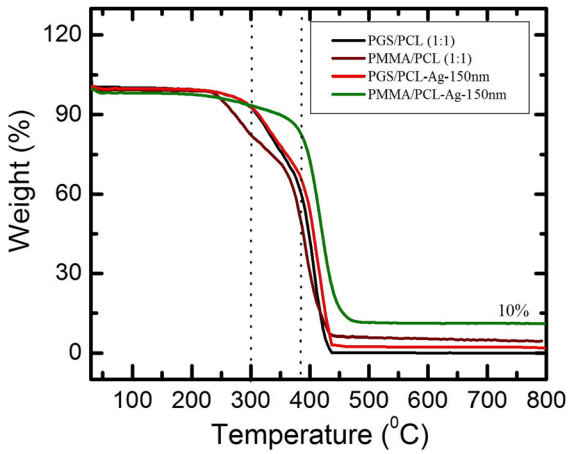

Fig. 8 Thermo gravimetric analysis (TGA) measurement was done for both pristine PGS/PCL, PMMA/PCL scaffolds and Ag-coated PGS/PCL, PMMA/PCL scaffolds under nitrogen atmosphere. The mass loss in fibers associated with burning fibrous scaffolds was reduced in Ag-coated scaffolds

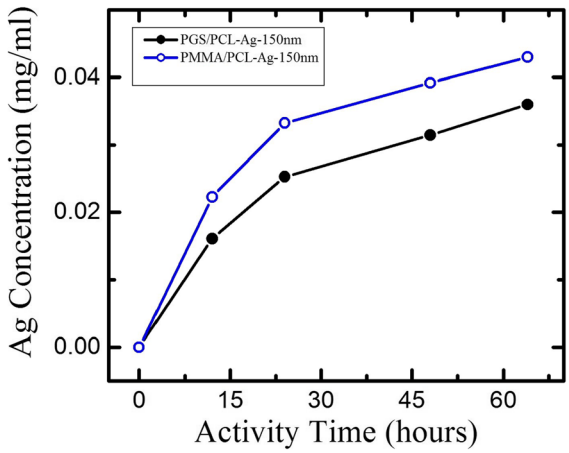

Fig. 9 Cumulative release of Ag + ion concentration of Ag-coated fibrous PGS/PCL and PMMA/PCL scaffolds in DI water as a function of time using ICP-OES

release of Ag + ions from the scaffolds, we employed the total immersion method in deionized (DI) water, a crucial investigation for understanding the anti-bacterial properties. The Ag-coated scaffolds were immersed in 2 ml of DI water for several days, and the concentration of Ag + ions was subsequently quantified using ICP-OES (Fig. 9). Notably, both Ag-coated scaffolds exhibited similar release profiles of Ag + ions, indicating a consistent trend (Fig. 8). Our analysis revealed that even after 3 days, approximately 5–10% of AgNPs was released, underscoring the substantial reservoir of AgNPs on the fiber surfaces [19, 51]. In our previous investigations, we observed that the release of Ag + ions escalates with an increase in the thickness of the Ag coating (10–15%). This observation highlights the need to evaluate the coating levels before assessing their anti-bacterial activity. We propose that the controlled release of Ag + ions from both scaffolds serves to mitigate potential toxicity concerns while effectively imparting anti-bacterial properties. Consequently, we emphasize that Ag-coated scaffolds hold immense promise across a spectrum of biomedical applications, including wound healing dressings, surgical meshes, and anti-bacterial sutures. This controlled release mechanism enhances their safety and efficacy, making them valuable assets in the field of medical materials.

Conclusion

In this study, we employed a combination of electrospinning and RF sputtering techniques to fabricate composite fibrous scaffolds coated with silver nanoparticles (AgNPs) using PGS/PCL and PMMA/PCL polymers. Our results indicate that while the scaffold structure underwent significant changes, the chemical characteristics and surface activity of the PGS, PCL, and PMMA polymers remained intact. The mechanical properties of the scaffolds were notably enhanced, likely due to increased friction between fibers following Ag-coating. Upon comparative analysis, it was revealed that the PMMA/PCL composite fibrous scaffolds exhibited superior mechanical properties, demonstrating an increased modulus (*E*) and ultimate tensile strength (UTS), along with reduced tensile strain compared to the PGS/PCL scaffold. This enhancement can be attributed to the interlocking of fibers, which prevents slippage and augments frictional forces between adjacent fibers. Moreover, the Ag + coating contributed to improved thermal stability by reducing mass loss during heating. Our controlled release studies demonstrated a steady release of Ag + ions from the coated scaffolds over time. This controlled release mechanism holds promise for various biomedical applications, including surgical meshes, bandages, and wound healing dressings, where the anti-bacterial properties of AgNPs

are highly beneficial. While other metal nanoparticles have been explored for wound dressings, AgNPs stand out due to their foldable behavior, a crucial attribute for effective wound dressing applications. In summary, the AgNP-coated PGS/PCL and PMMA/PCL composite scaffolds offer enhanced mechanical properties and hold great potential for diverse biomedical applications. Our future studies will delve into both in vitro and in vivo assessments, aiming to validate and further understand the performance and biocompatibility of these AgNP-coated scaffolds. These investigations will provide valuable insights into the practical applications and safety of the developed composite scaffolds in biomedical contexts.

Acknowledgements The authors would like to thank the Government City College (A), Osmania University, Hyderabad for utilizing facilities.

Author contribution Parvathalu Kalakonda: supervision and execution, writing—original draft and editing, and visualization. Shalini Thudumu and Sowjanya Laxmi: designing experiment and data collection. All the other authors were involved in various parts of discussion of the project.

Data availability Data is provided with the request.

Compliance with ethical standards

Conflict of interest The authors declare no competing interests.

References

1. Sen CK, Gordillo GM, Roy S, Kirsner R, Lambert L, Hunt TK, Longaker MT (2009) Wound Repair Regen 17(6):763–771
2. Atiyeh BS, Costagliola M, Hayek SN, Dibo SA (2007) Burns 33(2):139–148
3. Driver VR, Fabbi M, Lavery LA, Gibbons G (2010) J Vasc Surg 52(5):17S-22S
4. Branski LK, Gauglitz GG, Herndon DN, Jeschke MG (2009) Burns 35(2):171–180
5. Epstein FH, Singer AJ, Clark RA (1999) N Engl J Med 341(10):738–746
6. Bayram Y, Parlak M, Aypak C, Bayram I (2013) Int J Med Sci 10(1):19
7. Kanmani P, Rhim JW (2014) Food Chem 148:162–169
8. Zhang LL, Jiang YH, Ding YL, Daskalakis N, Jeuken L, Povey M, York DW (2010) J Nanoparticle Res 12:1625–1636
9. Arfat YA, Benjakul S, Prodpran T, Sumpavapol P, Songtipya P (2014) Food Hydrocoll 41:265–273
10. Kalakonda P, Banne S (2018) Plasmonics 13:1265–1269
11. Kalakonda P, Banne S (2017) Plasmonics 12(4):1221–1225
12. Kalakonda P (2016) Nanomater Nanotechnol 6
13. Hemar Y, Liu LH, Meunier N, Woonton BW (2010) Innov Food Sci Emerg Technol 11:432–440
14. Sheu MT, Huang JC, Yeh GC, Ho HO (2001) Biomaterials 22(15):1713–1719
15. Kong HJ, Wong E, Mooney DJ (2003) Macromolecules 36(12):4582–4588
16. Khademhosseini A, Vacanti JP, Langer R (2009) Sci Am 300:64–71
17. Radisic M, Park H, Martens TP, Salazar-Lazaro JE, Geng W, Wang Y, Vunjak-Novakovic G (2008) J Biomed Mater Res 86(3):713–724
18. Redenti S, Neeley WL, Rompani S, Saigal S, Yang J, Klassen H, Young MJ (2009) Biomaterials 30(21):3405–3414
19. Kalakonda P, Aldhahri MA, Abdelwahab MS, Tamayol A, Moghaddam KM, Ben Rached F, Chaieb S (2017) RSC Adv 7(55):34331–34338
20. Kalakonda P, Banne S (2017) Nanotechnol Sci Appl 10:45–53
21. Kalakonda P, Banne S, Kalakonda PB (2022) J Polym Res 29:442
22. Masoumi N, Larson BL, Annabi N, Kharaziha M, Zamanian B, Shapero KS, Khademhosseini A (2014) Adv Healthc Mater 3(6):929–939
23. Wang Y, Ameer GA, Sheppard BJ, Langer R (2002) Nat Biotechnol 20(6):602–606
24. Wang YD, Kim YM, Langer R (2003) J Biomed Mater Res A 66(1):192–197
25. Fidkowski C, Kaazempur-Mofrad MR, Borenstein J, Vacanti JP, Langer R, Wang Y (2005) Tissue Eng 11(2–3):302–309
26. Sundback CA, Shyu JY, Wang YD, Faquin WC, Langer RS, Vacanti JP, Hadlock TA (2005) Biomaterials 26(23):5454–5464
27. Khademhosseini A, Langer R, Borenstein J, Vacanti JP (2006) Proc Natl Acad Sci USA 103(7):2480–2487
28. Motlagh D, Yang J, Lui KY, Webb AR, Ameer GA (2006) Biomaterials 27(17):4315–4324
29. Catledge SA, Clem WC, Shrikishen N, Chowdhury S, Stanishevsky AV, Koopman M, Vohra YK (2007) Biomed Mater 2(3):142–150
30. Engelmayr GC, Cheng MY, Bettinger CJ, Borenstein JT, Langer R, Freed LE (2008) Nat Mater 7(11):1003–1010
31. Gao J, Crapo P, Nerem R, Wang YD (2008) J Biomed Mater Res A 85(4):1120–1128
32. Boland ED, Pawlowski KJ, Barnes CP, Simpson DG, Wnek GE, Bowlin GL (2006) ACS Symp Ser 918:188–204
33. Baker BM, Gee AO, Metter RB, Nathan AS, Marklein RA, Burdick JA, Mauck RL (2008) Biomaterials 29(9):2348–2358
34. Balguid A, Rubbens MP, Mol A, Bank RA, Bogers AJ, van Kats JP, Bouten CV (2007) Tissue Eng 13(7):1501–1511
35. Kim GH (2008) Biomed Mater 3(2):025010
36. Li C, Vepari C, Jin HJ, Kim HJ, Kaplan DL (2006) Biomaterials 27(16):3115–3124
37. Balguid A, Mol A, van Marion MH, Bank RA, Bouten CV, Baaijens FP (2009) Tissue Eng Part A 15(2):437–444

38. Almajhdi FN, Fouad H, Khalil KA, Awad HM, Mohamed SH, Elsarnagawy T, Abdo HS (2014) J Mater Sci: Mater Med 25(4):1045–1053
39. Chaubey N, Sahoo AK, Chattopadhyay A, Ghosh SS (2014) Biomater Sci 2(8):1080–1089
40. Gungor-Ozkerim PS, Balkan T, Kose GT, Sarac AS, Kok FN (2014) J Biomed Mater Res A 102(5):1897–1908
41. Jiang J, Xie J, Ma B, Bartlett DE, Xu A, Wang CH (2014) Acta Biomater 10(3):1324–1332
42. Wang H, Li Y, Jiang S, Zhang P, Min S, Jiang S (2014) J Appl Polym Sci 131(1):40903
43. Tseng YY, Liu SJ (2015) Nanomedicine 10:1785–1800
44. Kalakonda P, Kalakonda PB, Banne S (2021) Nanomater Nanotechnol 11
45. Kalakonda P, Cabrera Y, Judith R, Georgiev GY, Cebe P, Iannacchione GS (2014) MRS Online Proc Libr 1660:25–30
46. Kalakonda P, Daly J, Xu K, Georgiev GY, Cebe P, Iannacchione GS (2012) MRS Online Proc Libr 1499:583
47. Sant S, Iyer D, Gaharwar AK, Patel A, Khademhosseini A (2013) Acta Biomater 9(3):5963–5973
48. Iovits JL, Devlin JJ, Eng G, Martens TP, Vunjak-Novakovic G, Burdick JA (2009) ACS Appl Mater Interfaces 1(8):1878–1886
49. Iovits JL, Padera RF, Burdick JA (2008) Biomed Mater 3(3):034104
50. Sant S, Hwang CM, Lee SH, Khademhosseini A (2011) J Tissue Eng Regen Med 5(4):283–291
51. Qian G, Zhang L, Liu X, Shengda Wu, Peng S, Shuai C (2021) Mater Sci Eng, C 129:112425
52. Ferry JD (1980) Viscoelastic properties of polymers
53. Flory PJ, Rehner J (1943) Statistical mechanics of cross-linked polymer networks. J Chem Phys 11:512–520
54. Nielsen LE, Landel RF (1994) Mechanical properties of polymers and composites
55. Kalakonda P et al (2023) Facile Synthesis of Silver Nanoparticles Using Green Tea Leaf Extract and Evolution of Antibacterial Activity. Plasmonics 18:1837–1845
56. Kalakonda P et al (2023) Green synthesis and characteristics of silver nanoparticles using argyreia nervosa leaf extracts, and their antimicrobial activity. Plasmonic 18(3):1075–1081